Investigating the potential use of an oleaginous bacterium, *Rhodococcus opacus* PD630, for nano-TiO_2 remediation

*Archanaa Sundararaghavan[1], Amitava Mukherjee[2] and Gadi K. Suraishkumar[1]**

[1]Department of Biotechnology, Bhupat and Jyoti Mehta School of Biosciences building
Indian Institute of Technology Madras, Chennai 600036 India
[2]Centre for Nanobiotechnology, VIT University, Vellore 632 014 India

Author information

*Corresponding author

E–mail: gk@iitm.ac.in Phone: +91 44 2257 4105 Fax: +91 44 2257 4102

ORCID ID: 0000–0002–6521–4494

Acknowledgments

The authors thank the Sophisticated and Analytical Instrument Facility (SAIF, IITM, Chennai) for ICP–OES analysis and SEM analysis. The authors also thank the Environmental and Water Resource Engineering section of IIT Madras for help with size and zeta potential analyses.

Abstract

The occurrence of titanium dioxide nanoparticles ($nTiO_2$) in the effluents released from wastewater treatment plants, have raised concerns. The fate of $nTiO_2$ and their potential impact on organisms from different ecosystems are widely investigated. For the first time, in this work, we report the response of an oleaginous bacteria *Rhodococcus opacus* PD630, belonging to an ecologically important genus *Rhodococcus* to environmentally relevant concentrations of $nTiO_2$, under dark and UV light conditions. We observed a dose-dependent increase in $nTiO_2$ uptake by the bacteria that reached a maximum of 1.4 mg $nTiO_2$ (g cell)$^{-1}$ under mid-log UV exposure, corresponding to 97% uptake. The $nTiO_2$ induced oxidative stress in bacteria that increased from 25.1 to a maximum of 100.3, 44.1 and 51.7 µmol $\cdot OH$ (g cell)$^{-1}$ under dark, continuous and mid-log UV, respectively. However, $nTiO_2$ did not affect bacterial viability. Further, due to oxidative stress, the triacylglycerol (biodiesel) content from bacteria increased from 30% to a maximum of 54% CDW. Based on our findings, we propose an application of *R. opacus* PD 630 in $nTiO_2$ remediation due to their high $nTiO_2$ uptake and resistance.

Keywords: pollutants of concern; $nTiO_2$ release; wastewater treatment; oxidative stress; *R. opacus*; triacylglycerol

Introduction

Nano titanium dioxide ($nTiO_2$), an engineered nanoparticle (ENP), is widely used in various consumer products such as cosmetics, paint, textiles, and many others (Simonin et al. 2016; Noman et al. 2019). Their increased use has raised concerns on their environmental release and exposure and the adverse effects it could cause in the eco-system (Galletti et al. 2016; Bundschuh et al. 2018). The $nTiO_2$ eventually reach the wastewater treatment plant (WTP) through domestic usage, and their persistence in WTP effluent has been widely reported (Tong et al. 2015; Shi et al. 2016). Through effluent discharge or its reclamation for irrigation purposes, $nTiO_2$ enters the water bodies and soil ecosystems (Shi et al. 2016; Liu et al. 2018). Due to their prevalence in the environmental matrices, $nTiO_2$ are emerging as a contaminant of environmental concern (US EPA 2010; Simonin et al. 2016; Juliano and Magrini 2017; Qian et al. 2018).

The predicted $nTiO_2$ levels in the WTP's effluent range from 5 – 44 µg L^{-1} (Keller and Lazareva 2014; Sun et al. 2014b, 2016) and their actual measured values range from 10 – 100 µg L^{-1} (Kiser et al. 2009; Tong et al. 2015; Shi et al. 2016). However, the $nTiO_2$ concentration at which no adverse effect is expected on the ecosystem is 15.7 µg L^{-1} (Coll et al. 2016). The potential benefits of nanoparticles (NPs) are also associated with unknown risks (Singh 2016a). Risk characterization through exposure modeling shows $nTiO_2$ could be of marginal risk to organisms exposed to surface waters, but the risk is high to organism exposed to WTP effluents (Gottschalk et al. 2013; Semenzin et al. 2015).

The $nTiO_2$ cause harmful effects in living cells, by inducing oxidative stress through the generation of reactive species (RS) (Mathur et al. 2015; Bundschuh et al. 2018; Liu et al. 2018). At the environmentally relevant concentration (ERC) of 1, 10 and 100 µg L^{-1} $nTiO_2$ induced growth defects (Bar-Ilan et al. 2013), genotoxicity (Rocco et al. 2015) and reproductive defects in zebrafish (Wang et al. 2011), respectively. Field studies showed that $nTiO_2$ had negative effects on wheat growth and altered soil enzyme activities (Du et al. 2011), shortened life cycle

of *Arabidopsis thaliana* and altered soil microbial community (Liu et al. 2018). Further, field studies reported their accumulation in crucian carp (Shi et al. 2016), and studies conducted at ERC found $nTiO_2$ to accumulate in gills, guts, and ovaries of zebrafish (Wang et al. 2011; Bar-Ilan et al. 2013; Fang et al. 2016). Also, $nTiO_2$ gets trophically transferred across the food chain (Wang et al. 2011; Yeo and Nam 2013; Iswarya et al. 2018).

Several studies highlight the NP's toxic effects. However, their risk potential is uncertain and cannot be generalized as there are multiple factors such as size, shape, surface area, and many others that govern nanoparticles (NPs) behavior (Shang et al. 2014; Semenzin et al. 2015). There exists a knowledge gap regarding $nTiO_2$ fate (Adam et al. 2015) and hazard characterization, their uptake, and accumulation (Shang et al. 2014; Louie et al. 2016). Nevertheless, since a possibility of harm exists, it is worthwhile to develop proactive measures to reduce the risk, even if the ecological risk is not completely established (Singh 2016a, b).

Some techniques have been proposed for removal of emerging contaminants (ECs) from WTP effluent (Bilal et al. 2019). Biodegradation of ECs is considered effective (Bilal et al. 2019) and involves use of microbes (Ahmed et al. 2017; Men et al. 2017) and immobilized degradation enzymes (Bilal et al. 2019). However, NPs such as $nTiO_2$ are nonbiodegradable (Pulicharla et al. 2014). Possible application of membrane filtrations to prevent the release of NPs into the environment has been proposed (Ladner et al. 2012; Lee et al. 2017). However, frequent backwashing might be necessary to prevent membrane fouling, and washing the membrane would yet again result in NPs release (Olabarrieta et al. 2018; Zhang et al. 2019). Also, the membrane filtration process is energy-intensive and high cost associated (Ahmed et al. 2017).

Meanwhile, the biological filtration process using a crustacean *Daphnia magna* was found to be effective in removing ECs like pharmaceuticals from WTP effluent that was present in the range of ng L^{-1}(Matamoros et al. 2012). While a similar technology can be feasible for $nTiO_2$ removal,

it is important to identify an organism that is resistant to $nTiO_2$. We found only one study that had identified a bacterial strain, namely *Rhodococcus* strain GIN-1 that exhibited uniquely high resistance and strong adherence to bulk TiO_2 particles. The bacteria were employed for the recovery of TiO_2 from coal fly ash (CFA), a power plant generated waste (Shabtai and Fleminger 1994). Many years later, the same group had found the strong affinity of bacteria for $nTiO_2$ also (Gertler et al. 2003; Dayan et al. 2017). However, the effect of $nTiO_2$ particles, on the *Rhodococcus* bacteria especially at their ERC, has not been thoroughly characterized. Further, since the genus *Rhodococcus* is a strong inhabitant of contaminated soil and water and plays a major role in detoxifying them (Ivshina et al. 2019), it is important to study their response to new environmental stressors like $nTiO_2$.

In this study, the effects of $nTiO_2$ at their ERC, on the growth of a *Rhodococcus* bacteria were characterized, and $nTiO_2$ uptake efficiency by bacteria was quantified. Further, the genus *Rhodococcus* are oleaginous bacteria (Alvarez et al. 2013), and it is important to study the effect of $nTiO_2$ on their lipid (triacylglycerol or TAG, an important product) accumulation characteristics. Also, since $nTiO_2$ is a photocatalyst, the influence of UV light on its uptake and the eventual effect on growth and lipid accumulation were analyzed. The outcome of this research suggests the use of *Rhodococcus* bacteria to remediate $nTiO_2$ from the waste stream and contaminated environment.

Materials and Methods

Organism and culture

Rhodococcus opacus strain PD630 (Alvarez et al. 1996) was sourced from DSMZ (44193) culture collection, Germany. The strain *R. opacus* PD 630 was chosen because we wanted to study the $nTiO_2$ resistance and uptake on a species that accumulates a significant amount of triacylglycerol (TAG) (Alvarez et al. 2013). The culture maintenance and inoculum preparation

were carried out as reported in our earlier work (Archanaa et al. 2019). Since $nTiO_2$ adherence is maximum during the mid-log phase (Shabtai and Fleminger 1994) and as *R. opacus* PD630 accumulated maximum lipid in the mid-log phase (Archanaa et al. 2019), most of the measurements were based on the 12^{th} h (mid-log) sample, while a few studies such as the study of $nTiO_2$ effect on *R. opacus* PD630 growth, morphology and viability was done for an extended period. All experiments were carried out in triplicates and repeated on two other days to ensure reproducibility. One–way ANOVA was carried out using Megastat version 10.4.

R. opacus PD630 exposure to $nTiO_2$

To the study the effect of $nTiO_2$ on *R. opacus* PD630, the NB was spiked with different concentration of $nTiO_2$. The $nTiO_2$ concentration chosen for the study included 50 and 100 µg L^{-1} which were based on the levels reported in the WTP effluent (Kiser et al. 2009; Tong et al. 2015; Shi et al. 2016). Two higher $nTiO_2$ concentration of 200 and 1000 µg L^{-1} was also included in the study to characterize the high $nTiO_2$ exposure scenarios, resulting from its continuous discharge over a period or its accidental leakage from production sites. Also, the $nTiO_2$ concentrations range used in this work is representative of the levels found in secondary and primary effluents (Kiser et al. 2009; Westerhoff et al. 2011; Tong et al. 2015; Shi et al. 2016). The working $nTiO_2$ concentrations mentioned above were obtained by adding the appropriate volumes of $nTiO_2$ stock solution to the NB medium.

The $nTiO_2$ (anatase, <25 nm, Sigma–637254) stock solution was prepared (Online resource) based on the protocol of Kiser et al. (2009). The anatase was chosen as it is more photoactive and toxic when compared to rutile or brookite (Tong et al. 2015; De Matteis et al. 2016). The UVB (Ultraviolet B; Philips narrowband, TL 20W/01) light was used to induce photocatalysis of $nTiO_2$. The experiments were conducted in 500 ml conical flasks with 200 ml medium. The different conditions employed in the study are given in table 1. In the case of UVB treatment,

two different treatments were employed, as described in table 1. With a Lutron UV light meter, the intensity of UVB at the culture flask surface was measured to be 25 µW cm^{-2}. The media was inoculated with *R. opacus* PD 630 and maintained at 28 ˚C and 200 rpm

Particle size analysis of $nTiO_2$

The effective hydrodynamic diameter of $nTiO_2$, dispersed in the stock solution was measured through dynamic light scattering (DLS) using 90 plus Particle Size Analyser (Brookhaven Instruments Corporations, USA). Similarly, the effective hydrodynamic diameters of $nTiO_2$ at 50, 100, 200 and 1000 µg L^{-1}concentrations in NB were also measured. Further, the factors that can influence nanoparticle aggregation such as pH and ionic strength of the medium (He et al. 2015) was measured at 0^{th} h and 12^{th} h of growth. The pH was measured using a pH probe (pHspear, Eutech instruments) and ionic strength was obtained by measuring conductivity using a conductivity meter (PCTester 35, Eutech Instruments).

Zeta potential analysis

The zeta potential or surface charge of $nTiO_2$ in the stock solution was measured using nanoparticle size analyzer (SZ–100, Nanoparticle, Horiba, Germany). Similarly, the surface charges of $nTiO_2$ and *R. opacus* PD 630 in NB were measured using nanoparticle size analyzer.

FTIR analysis

The FT–IR analysis was performed for bacterial cells exposed to $nTiO_2$ and its cell lysate. Cells exposed to 1000 µg L^{-1} of $nTiO_2$ under dark, MUV and CUV for 12 h were harvested and lyophilized overnight. For lysate, cells exposed to 1000 µg L^{-1} of $nTiO_2$ under dark conditions for 12 h were harvested and resuspended in water. The cells in suspension were disrupted using a high-intensity probe sonicator (Qsonica Q700, Newton, CT, USA) for 5 min (each on/off pulse

cycle was 2 s) to release the intracellular content. The supernatant of the centrifuged cell lysate was collected and lyophilized. The dried cells and the intracellular contents were then analyzed by FT–IR (Spectrum one, PerkinElmer) spectroscopy by the KBr pellet method.

ICP-OES analysis

The $nTiO_2$ uptake by *R. opacus* PD 630 was quantified by measuring the elemental titanium (Ti) through inductively coupled plasma optical emission spectroscopy (ICP–OES). The cells were harvested by 12^{th} h and lyophilized. The dried biomass was acid digested with microwave-assistance (Multiwave 3000, Anton Paar, Graz, Austria) according to the established protocol (Nischwitz and Goenaga-Infante 2012). The elemental Ti produced from $nTiO_2$ through acid digestion was quantified by ICP–OES (Optima 5300DV, Perkin–Elmer Instruments, USA). From the measured Ti levels, equivalent levels of $nTiO_2$ were calculated. The $nTiO_2$ uptake was represented as specific uptake, i.e., mg $nTiO_2$ per g of biomass. The $nTiO_2$ uptake removed from the medium was calculated by dividing the amount of $nTiO_2$ uptaken with the initial amount of $nTiO_2$ provided in the media. The obtained fraction was converted into % uptake of $nTiO_2$.

Intracellular hydroxyl radical (oxidative stress) measurement

The fluorescent dye p–aminophenyl fluorescein (APF; Invitrogen™ Molecular Probes®, CA) was used to measure intracellular hydroxyl radical ($\cdot OH$) levels in *R. opacus* PD 630. Samples were harvested in the 12^{th} h and were normalized to 1 OD through resuspension in appropriate volumes. The protocol given by Setsukinai et al. (2003) was followed. To the cell suspension, APF was added to result in a final concentration of 10 µM. It was then incubated for 30 min at room temperature. A fluorimeter (LS55, PerkinElmer, Liantrisant, UK) was used for the fluorescence measurements at 490/515 nm excitation/emission in a 96-well plate.

Growth study

The growth assessment of bacteria and the growth rate calculation were carried out as reported in our previous work (Archanaa et al. 2019). The interference of $nTiO_2$ with OD measurements of cells, if any, was checked by adding different $nTiO_2$ concentrations to a particular cell concentration. The corresponding OD values were measured, which showed that the presence of $nTiO_2$ did not interfere with OD measurements at 600 nm (Fig. S1).

Cell viability assay

Cell viability assay or cytotoxic assay was done by assaying for Lactate dehydrogenase (LDH) released into the extracellular space, which is an indicator of membrane porosity or cytotoxicity resulting through nanoparticle interactions (Potter and Stern 2011). The culture filtrate from 12^{th} h and 24^{th} h for the samples treated with the highest $nTiO_2$ concentration of 1000 µg L^{-1}under dark, MUV, and CUV were used. The presence of LDH in the filtrate was checked according to a previously reported protocol (Howell et al. 1979). The cell lysate containing intracellular LDH obtained from any one of the samples was used as a positive control.

Cell morphology analysis

The morphology of bacteria with and without $nTiO_2$ exposure was observed through SEM. The cells treated with the highest $nTiO_2$ concentration of 1000 µg L^{-1} under dark, MUV, and CUV were used. The bacterial cells grown in respective NB were harvested from 12^{th} h and 24^{th} h of treatment and lyophilized overnight. The dried sample was prepared for SEM analysis in a sterile glass slide (Nagarajan et al. 2012), The instrument used was a FEI Quanta FEG 200 – High-Resolution Scanning Electron Microscope. The bacterial size was measured with SEM image analyzer.

TAG to biodiesel: conversion, quantification and fatty acid profiling

The TAGs were quantified by gravimetry – they were converted to fatty acid methyl esters (FAMEs) by *in situ* biomass transesterification, as reported in our previous work (Archanaa et al. 2019). The biodiesel was further characterized by calculating their physiochemical properties such as Iodine value (IV), cetane number (CN), density (ρ), viscosity (ν), and calorific value (CV) as reported in our previous study (Archanaa et al. 2018). The relative percentages of individual FAME components were calculated, and the variations in FAMEs were analysed by constructing a heat map using the tool ClustVis (Metsalu and Vilo 2015)

Results and discussion

A colloidally-stable $nTiO_2$ dispersion was employed

For in vitro or in vivo studies involving nanoparticles, unstable or agglomerated nanoparticle dispersions can lead to deceptive results (Moore et al. 2015) and hence we confirmed that the nanoparticles were effectively dispersed (Hasan Nia et al. 2015). While the original or primary size of the $nTiO_2$ particles as confirmed through SEM was < 25 nm, the effective hydrodynamic diameter (d_h) of $nTiO_2$ dispersed in ultrapure water as measured through DLS was 94 ± 19 nm. The increase in size indicted that $nTiO_2$ particles aggregated in aqueous solution. However, the zeta potential or surface charge of $nTiO_2$, dispersed in ultrapure water was measured to be –26.5 ± 2.7 mV, which indicated that the $nTiO_2$ formed reasonably stable colloidal aggregates; it is known that the zeta potential values greater than –30 mV indicate highly stable colloidal aggregates (Hasan Nia et al. 2015).

Similarly, the d_h of $nTiO_2$ in NB was also measured by DLS. The d_h for $nTiO_2$ concentration of 50, 100, 200, and 1000 µg L^{-1} was found to be 114 ± 10, 124 ± 13, 183 ± 15, 330 ± 27 nm respectively. The d_h of $nTiO_2$ in the NB increased with concentration and was larger when compared to that in water, as the aggregation of nanoparticles in biological media is a common

phenomenon (Park and Oh 2014; Guerrini et al. 2018). One of the possible reason could be the high ionic strength (Guerrini et al. 2018) of the nutrient medium (0.085 M). The aggregation can induce particle sedimentation and reduce the effective concentration of nanoparticles in contact with the cell (Sun et al. 2014). However, continuous shaking at high rpm (200 in this case) is known to prevent nanoparticles settling (Raychoudhury et al. 2010; Yu et al. 2015).

Further, while the nanoparticle aggregation in cell-free biological media increases with time, in the presence of growing cells, their aggregation behavior is different. The bacterial cells are known to aid in dispersing nanoparticles agglomerates and decrease their settling (Horst et al. 2010). Additionally, during the 12 h study period, no significant change in factors that can influence particle aggregation and settlings, such as pH (7.3 to 7.6) and Ionic strength (0.085 to 0.088) was observed.

R. opacus PD 630 attached and internalized $nTiO_2$

During NP exposure, attachment of NP on a cell's surface and internalization is a commonly observed phenomenon (Iswarya et al. 2015; Thiagarajan et al. 2019). The bacteria *R. opacus* PD630 was found to attach $nTiO_2$ onto them as shown by FT–IR spectroscopy. Bacteria when exposed to 1000 µg L^{-1} of $nTiO_2$, under dark, MUV and CUV, bands were observed in the fingerprint region (900–450 cm^{-1}) of the FT–IR spectrum, which was not present in control (Fig. 1). The bands observed in the region of 900–450 cm^{-1} especially from 700–450 cm^{-1} in case of $nTiO_2$ exposed cells corresponded to vibrations of Ti–O–Ti symmetric stretching (Enríquez et al. 2013; Iswarya et al. 2015) thus proving their attachment onto cells.

To better understand the nature of $nTiO_2$ binding to bacteria, the surface charges of bacteria and $nTiO_2$ in the NB were measured. The mean zeta potential of *R. opacus* PD 630 and $nTiO_2$ as measured by size analyzer was found to be –9.2 mV and –12.9 mV respectively, suggesting that the binding was not electrostatic (Dalai et al. 2014). A recent docking study conducted with

another species of *Rhodococcus,* also showed that the binding was not electrostatic, but coordinative (Dayan et al. 2017). However, the nature of interaction might be different in a natural environment as the NPs can undergo charge reversal, and many factors such as pH, IS, and natural organic matter (NOM) govern their surface charge (Li et al. 2016; Oriekhova and Stoll 2016).

Further, the ability of *R. opacus* PD 630 to internalize the $nTiO_2$ was confirmed by performing FT–IR analysis of the cell lysate. As discussed previously in this section, bands in the region of 900 – 450 cm^{-1} in FT–IR spectrum of the cell lysate (Fig. 1) show the presence of $nTiO_2$ in the intracellular space and thus confirm $nTiO_2$ internalization. Internalization of $nTiO_2$ in other bacteria and microalgae have also been reported (Bardaweel et al. 2018; Roy et al. 2018).

R. opacus PD 630 showed 97% uptake of $nTiO_2$ under the influence of MUV

The total $nTiO_2$ uptake by *R. opacus* PD 630, resulting from attachment and internalization, was quantified by ICP–OES. As seen from figure 2a, the specific $nTiO_2$ uptake increased with increasing concentration of $nTiO_2$ under dark, CUV, and MUV. The $nTiO_2$ was not detected in the control as expected (data not shown). The maximum difference in specific $nTiO_2$ uptake observed was with $nTiO_2$ concentration of 1000 µg L^{-1} across different conditions. The specific $nTiO_2$ uptake was 0.8 and 1.1 mg $(g\ cell)^{-1}$ under dark and CUV, respectively. The data suggested that exposure to CUV during the treatment process had a positive effect on the removal of $nTiO_2$ from the medium, as there was an increased specific $nTiO_2$ uptake under UV. Similar observations have been reported with few eco-toxicological studies, wherein exposure to UV during bacteria–nanoparticle interaction resulted in increased nanoparticle uptake, possibly due to increased membrane permeabilization (Dalai et al. 2014; Mathur et al. 2015). The corresponding percentage uptake of $nTiO_2$ by *R. opacus* PD 630 were 57 and 73% under dark and CUV, respectively (Fig. 2b).

Further, the positive effect of UV on $nTiO_2$ uptake was more pronounced, when the UV exposure was initiated from mid-log phase (MUV), rather than the continuous exposure. The specific $nTiO_2$ uptake under MUV for $nTiO_2$ concentration of 1000 µg L^{-1} increased to 1.4 mg (g cell)$^{-1}$ that corresponded to a percentage uptake of 97. Thus, recovery of $nTiO_2$ by *R. opacus* PD 630 was almost complete with UV light assistance. Similar to *R. ruber* (Dayan et al. 2017) originally isolated by Shatbai and Fleminger (1994), *R. opacus* PD 630 showed strong adherence for $nTiO_2$. Further, other than $nTiO_2$, *Rhodococcus* strain also shows a strong affinity for a few other metal oxides such as zinc oxide (ZnO) (Gertler et al. 2003). The accumulation of EC, such as NPs in one organism might reduce their exposure risk to other organisms in a contaminated environment (Liu et al. 2018).

$nTiO_2$ induced oxidative stress in *R. opacus* PD 630

One of the commonly observed responses in an organism, when exposed to nTiO2, is the induction of oxidative stress through the generation of RS (Marslin et al. 2017; Roy et al. 2018). Thus, induction of oxidative stress in *R. opacus* PD 630 via $nTiO_2$ exposure was studied by measuring intracellular levels of hydroxyl radicals ($\cdot OH$), the most reactive form of oxygen (Nita and Grzybowski 2016). Since UV light has been used in the study to induce photocatalysis of $nTiO_2$, the sole effect of UV on specific intracellular levels of $\cdot OH$ (si–OH) in *R. opacus* PD 630 was also studied because UV itself, can induce oxidative stress (Balan and Suraishkumar, 2014). However, no change was observed in si–OH levels in *R. opacus* PD 630 with either CUV or MUV when compared to control (Fig. S2).

Nevertheless, when $nTiO_2$ was present in the medium, a dose-dependent increase in si–OH levels were observed (Fig. 3). In the case of CUV, the increase in si–OH levels were 39, 50, 71 and 83% w.r.t control for $nTiO_2$ concentrations of 50, 100, 200 and 1000 µg L^{-1}, respectively. As observed with specific $nTiO_2$ uptake, the si–OH levels increased further, when UV exposure was

initiated from the mid-log phase. The increase in si–OH levels were 39, 69, 97 and 114% w.r.t control for $nTiO_2$ concentration of 50,100, 200 and 1000 µg L^{-1}, respectively.

While TiO_2 is known to induce oxidative stress under the influence of UV (Iswarya et al. 2015; Ripolles-Avila et al. 2019), TiO_2 itself can generate RS regardless of UV irradiation (Manzo et al. 2015; Thiagarajan et al. 2019). In support of this phenomenon, in the current study, we found that $nTiO_2$ uptake, in the absence of UV, induced oxidative stress in *R. opacus* PD 630 and a dose-dependent increase in si–OH levels were observed (Fig. 3). The increase in si–OH levels were 88, 122, 241 and 315% w.r.t control for $nTiO_2$ concentration of 50,100, 200 and 1000 µg L^{-1}, respectively. The increase in si–OH levels were predominant under dark, when compared to UV light which was surprising as $nTiO_2$ is expected to be catalytically more active in the presence of light (Roy et al. 2018; Ripolles-Avila et al. 2019). Possibly, the increased specific $nTiO_2$ uptake under UV exposure, as discussed in the previous section may have triggered certain defense systems to lower the oxidative stress levels, and further research is needed for a better understanding.

R. opacus PD 630 was resistant to $nTiO_2$ induced oxidative stress

The toxic nature of $nTiO_2$ is often attributed to its ability to increase RS generation in a cell (Manzo et al. 2015; Marslin et al. 2017). The resulting oxidative stress is known to damage the cell membrane and decreases cell viability (Mathur et al. 2015; Roy et al. 2018). However, the bacteria from the genus *Rhodococcus* survives in the most recalcitrant and toxic environment (Ivshina et al. 2019). In the current study, in spite of high $nTiO_2$ uptake and oxidative stress, no significant change in the growth of *R. opacus* PD 630 was observed when exposed to $nTiO_2$ for 24 hours, either under dark, CUV or MUV (Fig. S3) and the growth rates under all the conditions were comparable (Table S1).

Since optical density measurement cannot distinguish viable cells from dead cells, the cell viability was confirmed through LDH assay. The assay which showed a negligible change in absorbance at 340 nm (Fig. S4), suggested that there was no release of LDH into the extracellular space. The unchanged absorbance confirms that there was no appreciable loss in cell viability and membrane integrity. A positive control that contained LDH from cell lysate was maintained to confirm the results better.

The SEM analysis also showed no significant change in morphology of *R. opacus* PD 630 exposed to $nTiO_2$ for 24 hours, either under dark, CUV, or MUV (Fig. 4). There was no change in size either, as the dimensions of the bacteria exposed to $nTiO_2$ under dark, CUV or MUV were comparable to control both at 12^{th} h and 24^{th} h (Fig. 4). The above observations suggested *R. opacus* PD 630 was resistant to $nTiO_2$. In contrast to bacteria such as *Shewanella oneidensis* and a few other genera including *Escherichia*, *Staphylococcus*, *Lactobacillus*, *Salmonella*, which were found to be sensitive to $nTiO_2$ (100 µg L^{-1}) induced oxidative stress (Maurer-Jones et al. 2013; Ripolles-Avila et al. 2019), *R. opacus* PD 630 displayed resistance even at higher concentration $nTiO_2$ of 1000 µg L^{-1}. Since the bacteria was resistant to anatase which is, in general, more toxic than rutile (Tong et al. 2015; De Matteis et al. 2016), it is reasonable to expect their resistance to relatively less toxic rutile $nTiO_2$.

The resistance of *Rhodococcus* to ENP like $nTiO_2$ and their uptake is of significance since they are one of the major bacteria that colonize a biologically active filter (Zhang et al. 2018), which can be employed for tertiary treatment of effluent (Zhang et al. 2017) or in drinking water treatment facility for ECs removal (McKie et al. 2016).

The resistance of *R. opacus* PD 630 to $nTiO_2$ induced oxidative stress is indicated by the fact that it prefers the Entner–Doudoroff pathway for its catabolism (Hollinshead et al. 2016), which is considered as an important trait for tolerance to increased oxidative stress in certain soil bacteria (Chavarría et al. 2013).

Oxidative stress improved biodiesel production from *R. opacus* PD 630

RS that causes oxidative stress is known to have dual roles; both deleterious and beneficial based on their concentrations (Bardaweel et al. 2018). While considered harmful in general, oxidative stress has positively influenced the lipid accumulation in microalgae (Balan and Suraishkumar 2014; Fan et al. 2014). Similarly, oxidative stress induced by $nTiO_2$ in *R. opacus* PD 630 was found to improve TAG production concomitantly. As with oxidative stress, the sole effect of UV on the FAMEs content of *R. opacus* PD 630 was also studied and was observed to cause no change (Fig. S2). But with $nTiO_2$, dose-dependent increases in FAMEs content were observed under all conditions (Fig. 5a).

Under dark conditions, the FAMEs content increased by 17, 28, 43 and 60% w.r.t control for $nTiO_2$ concentration of 50,100, 200 and 1000 µg L^{-1}, respectively. Similarly, under CUV, the FAMEs content increased by 17, 32, 36 and 62% w.r.t control for $nTiO_2$ concentration of 50,100, 200 and 1000 µg L^{-1}, respectively. When UV irradiation was initiated from the mid-log phase, further improvement in FAMEs content was observed for 1000 µg L^{-1} $nTiO_2$. The percentage increase in FAMEs was found to be 8, 26, 42 and 81% w.r.t control for $nTiO_2$ concentration of 50,100, 200 and 1000 µg L^{-1}, respectively. Overall, a positive correlation was observed between FAMEs content and specific hydroxyl radical levels (Fig. 5b). However, for si–OH levels above 60 nmol (g cell)$^{-1}$, there was no significant improvement in FAMEs content with increasing si–OH levels, which implies that the beneficiary effects of RS are best observed if the levels are maintained below 60 nmol (g cell)$^{-1}$. The specific mechanism of RS in enhancing the lipid accumulation is not yet understood. However, as a secondary messenger, RS are believed to be an important mediator in carbon partitioning and lipid accumulation (Shi et al. 2017).

The findings indicated that apart from $nTiO_2$ uptake, a simultaneous increase in TAG (biodiesel) was also achieved. Thus, similar to microalgae which have been proposed for secondary

treatment of wastewater containing degradable ECs and biomass recovery (Matamoros et al. 2015), an integrated approach of $nTiO_2$ removal and biomass recovery for industrial application is a viable option.

Exposure of *R. opacus* PD 630 to $nTiO_2$ did not alter their native properties of biodiesel

The fatty acid properties such as chain length, composition, degree of saturation, etc., affect the biodiesel quality (Lamaisri et al. 2015; Kachel et al. 2018). The fatty acid composition of an oleaginous species changes with their culture conditions and any stress in the environment tend to alter their fatty acid profile (Minhas et al. 2016). Therefore, we studied the effect of $nTiO_2$ on the fatty acids profile produced by bacteria and on their final product quality. The list of general fatty acids obtained from the bacteria cultured under different conditions as analyzed through GC-MS is presented in table 2. The fatty acid chain length of the biodiesel ranged from C12 to C23; the degree of saturation was high. We did not observe poly–unsaturation in fatty acid chains.

The variations in individual fatty acid content across the samples were analyzed through a heat map (Fig. 6). Under all conditions, the major saturated fatty acids (SFAs) were palmitic acid (C16:0) and margaric acid (C17:0), and predominant monounsaturated fatty acids (MUFAs) included oleic acid (C18:1) and heptadecenoic acid (C17:1).

When compared to control, variations were observed in the relative content of certain fatty acids in other samples. The relative content of the SFA, C16:0 showed a decrease under certain conditions, especially for $nTiO_2$ exposure under dark, when compared to control. Whereas, the relative content of MUFAs when compared to control, increased for $nTiO_2$ exposure under dark. Thus, for $nTiO_2$ exposure under dark, the overall %SFAs significantly decreased, and %MUFAs significantly increased, while for others they were comparable to control (Fig. 7) with around 61% SFAs and 39% MUFAs. The increased percentage of unsaturation in *R. opacus* PD 630,

when exposed to $nTiO_2$ under dark can be a defense strategy against their higher si–OH levels (Yu et al. 2015).

Fortunately, the variations observed in the relative percentage of certain fatty acids across the samples were not significant enough to cause significant changes in certain biodiesel properties such as Iodine value (IV), cetane number (CN), density (ρ), viscosity (ν), and calorific value (CV) (Fig. S5). Values of all the properties were highly comparable between control and other samples. Further, their values were in accordance with already established Indian and international standards, and comparable to conventional petroleum diesel. The unaltered fuel properties showed that the quality of biodiesel is not affected (Qi et al. 2019) by *R. opacus* PD630 exposure to $nTiO_2$. The finding is of significance if *Rhodococcus* is employed for a coupled process of NP release mitigation and valuable metabolite production.

Conclusion

This work showed that the bacteria, *R. opacus* PD630 belonging to the genus *Rhodococcus* that predominantly inhabits the contaminated water and soil, was resistant to $nTiO_2$, a new class of environmental pollutant. While bacteria are known to attach, internalize, and uptake NPs when exposed to them, the *Rhodococcus* bacteria seem superior because of their high uptake and unique resistance to RS induced by $nTiO_2$. In addition to $nTiO_2$ uptake, the bacteria accumulate TAG, and the accumulation is further increased by $nTiO_2$-induced oxidative stress.

Funding

The authors thank the Department of Science and Technology (DST, grant no. SB/S3/CE/007/2013), and Department of Biotechnology (DBT, grant ref. No. BT/PR11328/PBD/26/176/2008), Government of India, for financial assistance.

Compliance with ethical standards

Conflict of Interest: The authors declare that they have no conflict of interest.

Ethical approval: This article does not contain any studies with human participants or animals performed by any of the authors.

FIGURE CAPTIONS

Fig. 1: FT-IR spectrum of Control and *R. opacus* PD 630 exposed to $nTiO_2$ concentration of 1000 µg L^{-1}under dark, CUV, and MUV. Bands in the fingerprint region (900-450 cm^{-1}) of samples exposed to $nTiO_2$ and its cell lysate confirmed the attachment and internalization of $nTiO_2$ respectively

Fig. 2: Specific $nTiO_2$ uptake (a) and % uptake (b) from media by *R. opacus* PD 630 under dark, CUV, and MUV. A dose-dependent increase in specific uptake and %removal was observed, with MUV showing maximum $nTiO_2$ removal of 97%. Data points are represented as mean ± SD, n = 3

Fig. 3: Specific intracellular levels of hydroxyl radicals in *R. opacus* PD 630 when exposed to $nTiO_2$ under dark, CUV, and MUV. A dose-dependent increase in si-OH levels was observed under all conditions, with dark conditions showing a maximum increase. Data points are represented as mean ± SD, n = 3. $^{*}p<0.01$, $^{**}p<0.05$, $^{***}p<0.005$

Fig. 4: Scanning electron micrographs of *R. opacus* PD 630, when exposed to 1000 µg $L^{-1}$of $nTiO_2$ under dark, CUV, MUV. Cell size is represented as Length X Width (µm). No appreciable change in morphology was observed

Fig. 5: FAME content of *R. opacus* PD 630 when exposed to $nTiO_2$ under dark, CUV, and MUV (a). A dose-dependent increase in FAME content was observed under all conditions, with MUV exposure showing a maximum increase. A positive correlation was observed between oxidative stress (si-OH levels) and FAME content in *R. opacus* PD 630 (b). Data points are represented as mean ± SD, n = 3. $^{*}p<0.01$, $^{**}p<0.05$, $^{***}p<0.005$

Fig. 6: Heat map of the relative percentage of individual FAMEs in biodiesel of *R. opacus* PD 630 when exposed to $nTiO_2$ under dark, CUV and MUV. When compared to control, variations were observed in C16:0 and C17:1, under other conditions

Fig. 7: Relative percentage of SFAs and MUFAs of biodiesel from *R. opacus* PD 630 when exposed to $nTiO_2$ under dark, CUV, and MUV. When compared to control, the %SFAs decreased, and %MUFAs increased for $nTiO_2$ exposure under dark conditions. Data points are represented as mean ± SD, n = 3. $^{**}p<0.05$, $^{***}P<0.005$

References

Adam V, Loyaux-Lawniczak S, Quaranta G (2015) Characterization of engineered TiO_2 nanomaterials in a life cycle and risk assessments perspective. Environ Sci Pollut Res 22:11175–11192. doi: 10.1007/s11356-015-4661-x

Ahmed MB, Zhou JL, Ngo HH, et al (2017) Progress in the biological and chemical treatment technologies for emerging contaminant removal from wastewater: A critical review. J Hazard Mater 323:274–298. doi: 10.1016/j.jhazmat.2016.04.045

Alvarez HM, Mayer F, Fabritius D, Steinbüchel A (1996) Formation of intracytoplasmic lipid inclusions by *Rhodococcus opacus* strain PD630. Arch Microbiol 165:377–386. doi: 10.1007/s002030050341

Alvarez HM, Roxana AS, Herrero M, et al (2013) Metabolism of triacylglycerols in *Rhodococcus* species: insights from physiology and molecular genetics. J Mol Biochem 2:69–78

Archanaa S, Jose S, Mukherjee A, Suraishkumar GK (2019) Sustainable Diesel Feedstock: a Comparison of Oleaginous Bacterial and Microalgal Model Systems. Bioenergy Res 12:205–216. doi: 10.1007/s12155-018-9948-6

Balan R, Suraishkumar GK (2014) Simultaneous increases in specific growth rate and specific lipid content of *Chlorella vulgaris* through UV-induced reactive species. Biotechnol Prog 30:291–299. doi: 10.1002/btpr.1854

Bar-Ilan O, Chuang CC, Schwahn DJ, et al (2013) TiO_2 nanoparticle exposure and illumination during zebrafish development: Mortality at parts per billion concentrations. Environ Sci Technol 47:4726–4733. doi: 10.1021/es304514r

Bardaweel SK, Gul M, Alzweiri M, et al (2018) Reactive oxygen species: The dual role in physiological and pathological conditions of the human body. Eurasian J Med 50:193–201. doi: 10.5152/eurasianjmed.2018.17397

Bilal M, Adeel M, Rasheed T, et al (2019) Emerging contaminants of high concern and their enzyme-assisted biodegradation – A review. Environ Int 124:336–353. doi: 10.1016/j.envint.2019.01.011

Bundschuh M, Filser J, Lüderwald S, et al (2018) Nanoparticles in the environment: where do we come from, where do we go to? Environ Sci Eur 30:1–17. doi: 10.1186/s12302-018-0132-6

Chavarría M, Nikel PI, Pérez-Pantoja D, De Lorenzo V (2013) The Entner-Doudoroff pathway empowers *Pseudomonas putida* KT2440 with a high tolerance to oxidative stress. Environ Microbiol 15:1772–1785. doi: 10.1111/1462-2920.12069

Coll C, Notter D, Gottschalk F, et al (2016) Probabilistic environmental risk assessment of five nanomaterials (nano-TiO_2, nano-Ag, nano-ZnO, CNT, and fullerenes). Nanotoxicology 10:436–444. doi: 10.3109/17435390.2015.1073812

Dalai S, Pakrashi S, Chakravarty S, et al (2014) Studies on interfacial interactions of TiO_2 nanoparticles with bacterial cells under light and dark conditions. Bull Mater Sci 37:371–381. doi: 10.1007/s12034-014-0680-3

Dayan A, Babin G, Ganoth A, et al (2017) The involvement of coordinative interactions in the binding of dihydrolipoamide dehydrogenase to titanium dioxide—Localization of a putative binding site. J Mol Recognit 30:1–11. doi: 10.1002/jmr.2617

De Matteis V, Cascione M, Brunetti V, et al (2016) Toxicity assessment of anatase and rutile titanium dioxide nanoparticles: The role of degradation in different pH conditions and light exposure. Toxicol Vitr 37:201–210. doi: 10.1016/j.tiv.2016.09.010

Du W, Sun Y, Ji R, et al (2011) TiO_2 and ZnO nanoparticles negatively affect wheat growth and soil enzyme activities in agricultural soil. J Environ Monit 13:822–828. doi: 10.1039/c0em00611d

Enríquez JMH, Lajas LAC, Alamilla RG, et al (2013) Synthesis of Solid Acid Catalysts Based

on TiO_2- $SO_4^{2-}$and Pt/TiO_2- SO_4^{2-} Applied in n-Hexane Isomerization. J Met 3:34–44. doi: http://dx.doi.org/10.4236/ojmetal.2013.33006

Fan J, Cui Y, Wan M, et al (2014) Lipid accumulation and biosynthesis genes response of the oleaginous *Chlorella pyrenoidosa* under three nutrition stressors. Biotechnol Biofuels 7:17. doi: 10.1186/1754-6834-7-17

Fang Q, Shi Q, Guo Y, et al (2016) Enhanced Bioconcentration of Bisphenol A in the Presence of Nano-TiO_2 Can Lead to Adverse Reproductive Outcomes in Zebrafish. Environ Sci Technol 50:1005–1013. doi: 10.1021/acs.est.5b05024

Galletti A, Seo S, Joo SH, et al (2016) Effects of titanium dioxide nanoparticles derived from consumer products on the marine diatom *Thalassiosira pseudonana*. Environ Sci Pollut Res 23:21113–21122. doi: 10.1007/s11356-016-7556-6

Gertler G, Brudo I, Kenig R, Fleminger G (2003) A TiO_2-Binding Protein isolated from *Rhodococcus* Strain GIN-1 (NCIMB 40340) - Purification, Properties and Potential Applications. Materwiss Werksttech 34:1138–1144. doi: 10.1002/mawe.200300709

Gottschalk F, Kost E, Nowack B (2013) Engineered nanomaterials in water and soils: A risk quantification based on probabilistic exposure and effect modeling. Environ Toxicol Chem 32:1278–1287. doi: 10.1002/etc.2177

Guerrini L, Alvarez-Puebla RA, Pazos-Perez N (2018) Surface modifications of nanoparticles for stability in biological fluids. Materials (Basel) 11:1–28. doi: 10.3390/ma11071154

Hasan Nia M, Rezaei-Tavirani M, Nikoofar AR, et al (2015) Stabilizing and dispersing methods of TiO_2 nanoparticles in biological studies. J Paramed Sci Spring 6:2008–4978

He G, Chen R, Lu S, et al (2015) Dominating Role of Ionic Strength in the Sedimentation of Nano-TiO_2 in Aquatic Environments. J Nanomater 2015:1–10. doi: 10.1155/2015/851928

Hollinshead WD, Henson WR, Abernathy M, et al (2016) Rapid metabolic analysis of *Rhodococcus opacus* PD630 via parallel13C-metabolite fingerprinting. Biotechnol Bioeng

113:91–100. doi: 10.1002/bit.25702

Horst AM, Neal AC, Mielke RE, et al (2010) Dispersion of TiO_2 nanoparticle agglomerates by *Pseudomonas aeruginosa*. Appl Environ Microbiol 76:7292–7298. doi: 10.1128/AEM.00324-10

Howell BF, McCune S, Schaffer R (1979) Lactate-to-pyruvate or pyruvate-to-lactate assay for lactate dehydrogenase: A re-examination. Clin Chem 25:269–272. doi: 10.1093/jac/dkr570

Hu Q, Sommerfeld M, Jarvis E, et al (2008) Microalgal triacylglycerols as feedstocks for biofuel production: Perspectives and advances. Plant J 54:621–639. doi: 10.1111/j.1365-313X.2008.03492.x

Iswarya V, Bhuvaneshwari M, Alex SA, et al (2015) Combined toxicity of two crystalline phases (anatase and rutile) of Titania nanoparticles towards freshwater microalgae: *Chlorella* sp. Aquat Toxicol 161:154–169. doi: 10.1016/j.aquatox.2015.02.006

Iswarya V, Bhuvaneshwari M, Chandrasekaran N, Mukherjee A (2018) Trophic transfer potential of two different crystalline phases of TiO_2 NPs from *Chlorella* sp. to *Ceriodaphnia dubia*. Aquat Toxicol 197:89–97. doi: 10.1016/j.aquatox.2018.02.003

Ivshina IB, Tyumina EA, Kuzmina M V, Vikhareva E V (2019) Features of diclofenac biodegradation by *Rhodococcus ruber* IEGM 346. Sci Rep 9:1–13. doi: 10.1038/s41598-019-45732-9

Juliano C, Magrini G (2017) Cosmetic Ingredients as Emerging Pollutants of Environmental and Health Concern. A Mini-Review. Cosmetics 4:11. doi: 10.3390/cosmetics4020011

Kachel M, Matwijczuk A, Przywara A, et al (2018) Profile of Fatty Acids and Spectroscopic Characteristics of Selected Vegetable Oils Extracted by Cold Maceration. Agric Eng 22:61–71. doi: 10.1515/agriceng-2018-0006

Kashmiri ZN, Mankar SA (2014) Free radicals and oxidative stress in bacteria. Int J Curr Microbiol Appl Sci 3:34–40

Keller AA, Lazareva A (2014) Predicted Releases of Engineered Nanomaterials: From Global to Regional to Local. Environ Sci Technol Lett 1:65–70. doi: 10.1021/ez400106t

Kiser MA, Westerhoff P, Benn T, et al (2009) Titanium nanomaterial removal and release from wastewater treatment plants. Environ Sci Technol 43:6757–6763. doi: 10.1021/es901102n

Ladner DA, Steele M, Weir A, et al (2012) Functionalized nanoparticle interactions with polymeric membranes. J Hazard Mater 211–212:288–295. doi: 10.1016/j.jhazmat.2011.11.051

Lamaisri C, Punsuvon V, Chanprame S, et al (2015) Relationship between fatty acid composition and biodiesel quality for nine commercial palm oils. Songklanakarin J Sci Technol 37:389–395

Lee H, Segets D, Süß S, et al (2017) Liquid filtration of nanoparticles through track-etched membrane filters under unfavorable and different ionic strength conditions: Experiments and modeling. J Memb Sci 524:682–690. doi: 10.1016/j.memsci.2016.11.023

Li L, Sillanpää M, Risto M (2016) Influences of water properties on the aggregation and deposition of engineered titanium dioxide nanoparticles in natural waters. Environ Pollut 219:132–138. doi: 10.1016/j.envpol.2016.09.080

Liu J, Williams PC, Geisler-Lee J, et al (2018) Impact of wastewater effluent containing aged nanoparticles and other components on biological activities of the soil microbiome, Arabidopsis plants, and earthworms. Environ Res 164:197–203. doi: 10.1016/j.envres.2018.02.006

Louie SM, Dale AL, Casman EA, Lowry G V (2016) Challenges Facing the Environmental Nanotechnology Research Enterprise. In: Xing B, Vecitis CD, Senesi N (eds) Engineered Nanoparticles and the Environment: Biophysicochemical Processes and Toxicity. John Wiley & Sons, Inc., Hoboken, New Jersey, pp 3–19

Manzo S, Buono S, Rametta G, et al (2015) The diverse toxic effect of SiO2 and TiO2

nanoparticles toward the marine microalgae *Dunaliella tertiolecta*. Environ Sci Pollut Res 22:15941–15951. doi: 10.1007/s11356-015-4790-2

Marslin G, Sheeba CJ, Franklin G (2017) Nanoparticles Alter Secondary Metabolism in Plants via ROS Burst. Front Plant Sci 8:1–8. doi: 10.3389/fpls.2017.00832

Matamoros V, Gutiérrez R, Ferrer I, et al (2015) Capability of microalgae-based wastewater treatment systems to remove emerging organic contaminants: A pilot-scale study. J Hazard Mater 288:34–42. doi: 10.1016/j.jhazmat.2015.02.002

Matamoros V, Sala L, Salvadó V (2012) Evaluation of a biologically-based filtration water reclamation plant for removing emerging contaminants: A pilot plant study. Bioresour Technol 104:243–249. doi: 10.1016/j.biortech.2011.11.036

Mathur A, Raghavan A, Chaudhury P, et al (2015) Cytotoxicity of titania nanoparticles towards waste water isolate *Exiguobacterium acetylicum* under UVA, visible light and dark conditions. J Environ Chem Eng 3:1837–1846. doi: 10.1016/j.jece.2015.06.026

Maurer-Jones MA, Gunsolus IL, Murphy CJ, Haynes CL (2013) Toxicity of engineered nanoparticles in the environment. Anal Chem 85:3036–3049. doi: 10.1021/ac303636s

McKie MJ, Andrews SA, Andrews RC (2016) Conventional drinking water treatment and direct biofiltration for the removal of pharmaceuticals and artificial sweeteners: A pilot-scale approach. Sci Total Environ 544:10–17. doi: 10.1016/j.scitotenv.2015.11.145

Men Y, Achermann S, Helbling DE, et al (2017) Relative contribution of ammonia oxidizing bacteria and other members of nitrifying activated sludge communities to micropollutant biotransformation. Water Res 109:217–226. doi: 10.1016/j.watres.2016.11.048

Metsalu T, Vilo J (2015) ClustVis: A web tool for visualizing clustering of multivariate data using Principal Component Analysis and heatmap. Nucleic Acids Res 43:W566–W570. doi: 10.1093/nar/gkv468

Minhas AK, Hodgson P, Barrow CJ, Adholeya A (2016) A review on the assessment of stress

conditions for simultaneous production of microalgal lipids and carotenoids. Front Microbiol 7:1–19. doi: 10.3389/fmicb.2016.00546

Moore TL, Rodriguez-Lorenzo L, Hirsch V, et al (2015) Nanoparticle colloidal stability in cell culture media and impact on cellular interactions. Chem Soc Rev 44:6287–6305. doi: 10.1039/c4cs00487f

Nagarajan AJ, Irusappan S, Amarnath G, et al (2012) Expeditious Synthesis of Silver Nanoparticles By A Novel Strain *Sporosarcina pasteurii* SRMNP1 and Patrocladogram Analysis For Exploration of its Closely Related Species. Int J Sci Res 3:63–65. doi: 10.15373/22778179/FEB2014/45

Nischwitz V, Goenaga-Infante H (2012) Improved sample preparation and quality control for the characterisation of titanium dioxide nanoparticles in sunscreens using flow field flow fractionation on-line with inductively coupled plasma mass spectrometry. J Anal At Spectrom 27:1084–1092. doi: 10.1039/c2ja10387g

Nita M, Grzybowski A (2016) The Role of the Reactive Oxygen Species and Oxidative Stress in the Pathomechanism of the Age-Related Ocular Diseases and Other Pathologies of the Anterior and Posterior Eye Segments in Adults. Oxid Med Cell Longev 2016:3164734. doi: 10.1155/2016/3164734

Noman MT, Ashraf MA, Ali A (2019) Synthesis and applications of nano-TiO_2: a review. Environ Sci Pollut Res 26:3262–3291. doi: 10.1007/s11356-018-3884-z

Olabarrieta J, Monzón O, Belaustegui Y, et al (2018) Removal of TiO_2 nanoparticles from water by low pressure pilot plant filtration. Sci Total Environ 618:551–560. doi: 10.1016/j.scitotenv.2017.11.003

Oriekhova O, Stoll S (2016) Stability of uncoated and fulvic acids coated manufactured CeO_2 nanoparticles in various conditions: From ultrapure to natural Lake Geneva waters. Sci Total Environ 562:327–334. doi: 10.1016/j.scitotenv.2016.03.184

Park JH, Oh N (2014) Endocytosis and exocytosis of nanoparticles in mammalian cells. Int J Nanomedicine 9:51–63. doi: 10.2147/ijn.s26592

Potter TM, Stern ST (2011) Evaluation of Cytotoxicity of Nanoparticulate Materials in Porcine Kidney Cells and Human Hepatocarcinoma Cells. Methods Mol Biol 697:157–165. doi: 10.1007/978-1-60327-198-1_16

Pulicharla R, Zolfaghari M, Brar SK, et al (2014) Cosmetic Nanomaterials in Wastewater: Titanium Dioxide and Fullerenes. J Hazardous, Toxic, Radioact Waste 20:B4014005. doi: 10.1061/(asce)hz.2153-5515.0000261

Qi F, Pei H, Mu R, et al (2019) Characterization and optimization of endogenous lipid accumulation in Chlorella vulgaris SDEC-3M ability to rapidly accumulate lipid for reversing nightly lipid loss. Biotechnol Biofuels 12:1–11. doi: 10.1186/s13068-019-1493-9

Qian J, Li K, Wang P, et al (2018) Unraveling adsorption behavior and mechanism of perfluorooctane sulfonate (PFOS) on aging aquatic sediments contaminated with engineered nano-TiO_2. Environ Sci Pollut Res 25:17878–17889. doi: 10.1007/s11356-018-1984-4

Raychoudhury T, Naja G, Ghoshal S (2010) Assessment of transport of two polyelectrolyte-stabilized zero-valent iron nanoparticles in porous media. J Contam Hydrol 118:143–151. doi: 10.1016/j.jconhyd.2010.09.005

Ripolles-Avila C, Martinez-Garcia M, Hascoët A-S, Rodríguez-Jerez JJ (2019) Bactericidal efficacy of UV activated TiO_2 nanoparticles against Gram-positive and Gram-negative bacteria on suspension. CyTA - J Food 17:408–418. doi: 10.1080/19476337.2019.1590461

Rocco L, Santonastaso M, Mottola F, et al (2015) Genotoxicity assessment of TiO_2 nanoparticles in the teleost *Danio rerio*. Ecotoxicol Environ Saf 113:223–230. doi: 10.1016/j.ecoenv.2014.12.012

Roy B, Chandrasekaran H, Palamadai Krishnan S, et al (2018) UVA pre-irradiation to P25 titanium dioxide nanoparticles enhanced its toxicity towards freshwater algae *Scenedesmus obliquus*. Environ Sci Pollut Res 25:16729–16742. doi: 10.1007/s11356-018-1860-2

Semenzin E, Lanzellotto E, Hristozov D, et al (2015) Species sensitivity weighted distribution for ecological risk assessment of engineered nanomaterials: The n-TiO_2 case study. Environ Toxicol Chem 34:2644–2659. doi: 10.1002/etc.3103

Setsukinai K, Urano Y, Kakinuma K, et al (2003) Development of novel fluorescence probes that can reliably detect reactive oxygen species and distinguish specific species. J Biol Chem 278:3170–3175. doi: 10.1074/jbc.M209264200

Shabtai Y, Fleminger G (1994) Adsorption of *Rhodococcus* strain GIN-1 (NCIMB 40340) on titanium dioxide and coal fly ash particles. Appl Environ Microbiol 60:3079–3088

Shang L, Nienhaus K, Nienhaus GU (2014) Engineered nanoparticles interacting with cells: Size matters. J Nanobiotechnology 12:1–12. doi: 10.1186/1477-3155-12-5

Shi K, Gao Z, Shi T-Q, et al (2017) Reactive Oxygen Species-Mediated Cellular Stress Response and Lipid Accumulation in Oleaginous Microorganisms: The State of the Art and Future Perspectives. Front Microbiol 8:1–9. doi: 10.3389/fmicb.2017.00793

Shi X, Li Z, Chen W, et al (2016) Fate of TiO_2 nanoparticles entering sewage treatment plants and bioaccumulation in fish in the receiving streams. NanoImpact 3–4:96–103. doi: 10.1016/j.impact.2016.09.002

Simonin M, Richaume A, Guyonnet JP, et al (2016) Titanium dioxide nanoparticles strongly impact soil microbial function by affecting archaeal nitrifiers. Sci Rep 6:1–10. doi: 10.1038/srep33643

Singh AK (2016a) The Past, Present, and the Future of Nanotechnology. Eng Nanoparticles 515–525. doi: 10.1016/b978-0-12-801406-6.00010-8

Singh AK (2016b) Introduction to Nanoparticles and Nanotoxicology. Eng Nanoparticles 1–18.

doi: 10.1016/b978-0-12-801406-6.00001-7

Sun M, Yu Q, Hu M, et al (2014a) Lead sulfide nanoparticles increase cell wall chitin content and induce apoptosis in *Saccharomyces cerevisiae*. J Hazard Mater 273:7–16. doi: 10.1016/j.jhazmat.2014.03.008

Sun TY, Bornhöft NA, Hungerbühler K, Nowack B (2016) Dynamic Probabilistic Modeling of Environmental Emissions of Engineered Nanomaterials. Environ Sci Technol 50:4701–4711. doi: 10.1021/acs.est.5b05828

Sun TY, Gottschalk F, Hungerbühler K, Nowack B (2014b) Comprehensive probabilistic modelling of environmental emissions of engineered nanomaterials. Environ Pollut 185:69–76. doi: 10.1016/j.envpol.2013.10.004

Thiagarajan V, Ramasubbu S, Natarajan C, Mukherjee A (2019) Differential sensitivity of marine algae *Dunaliella salina* and *Chlorella* sp. to P25 TiO2 NPs. Environ Sci Pollut Res 4:21394–21403. doi: 10.1007/s11356-019-05332-6

Tong T, Hill AN, Alsina MA, et al (2015) Spectroscopic characterization of TiO*2* polymorphs in wastewater treatment and sediment samples. Environ Sci Technol Lett 2:12–18. doi: 10.1021/ez5004023

US EPA (2010) Emerging Contaminants – Nanomaterials At a Glance. Environmental Protection Agency, USA

Wang J, Zhu X, Zhang X, et al (2011) Disruption of zebrafish (*Danio rerio*) reproduction upon chronic exposure to TiO2 nanoparticles. Chemosphere 83:461–467. doi: 10.1016/j.chemosphere.2010.12.069

Westerhoff P, Song G, Hristovski K, Kiser MA (2011) Occurrence and removal of titanium at full scale wastewater treatment plants: implications for TiO_2 nanomaterials. J Environ Monit 13:1195–1203. doi: 10.1039/c1em10017c

Yeo MK, Nam DH (2013) Influence of different types of nanomaterials on their bioaccumulation

in a paddy microcosm: A comparison of TiO_2 nanoparticles and nanotubes. Environ Pollut 178:166–172. doi: 10.1016/j.envpol.2013.03.040

Yu Q, Liu Z, Xu H, et al (2015) TiO_2 nanoparticles promote the production of unsaturated fatty acids (UFAs) fighting against oxidative stress in Pichia pastoris. RSC Adv 5:41033–41040. doi: 10.1039/C5RA02366A

Zhang M, Yang J, Cai Z, et al (2019) Detection of engineered nanoparticles in aquatic environments: Current status and challenges in enrichment, separation, and analysis. Environ Sci Nano 6:709–735. doi: 10.1039/c8en01086b

Zhang S, Courtois S, Gitungo S, et al (2018) Microbial community analysis in biologically active filters exhibiting efficient removal of emerging contaminants and impact of operational conditions. Sci Total Environ 640–641:1455–1464. doi: 10.1016/j.scitotenv.2018.06.027

Zhang S, Gitungo SW, Axe L, et al (2017) Biologically active filters – An advanced water treatment process for contaminants of emerging concern. Water Res 114:31–41. doi: 10.1016/j.watres.2017.02.014

Fig. 1

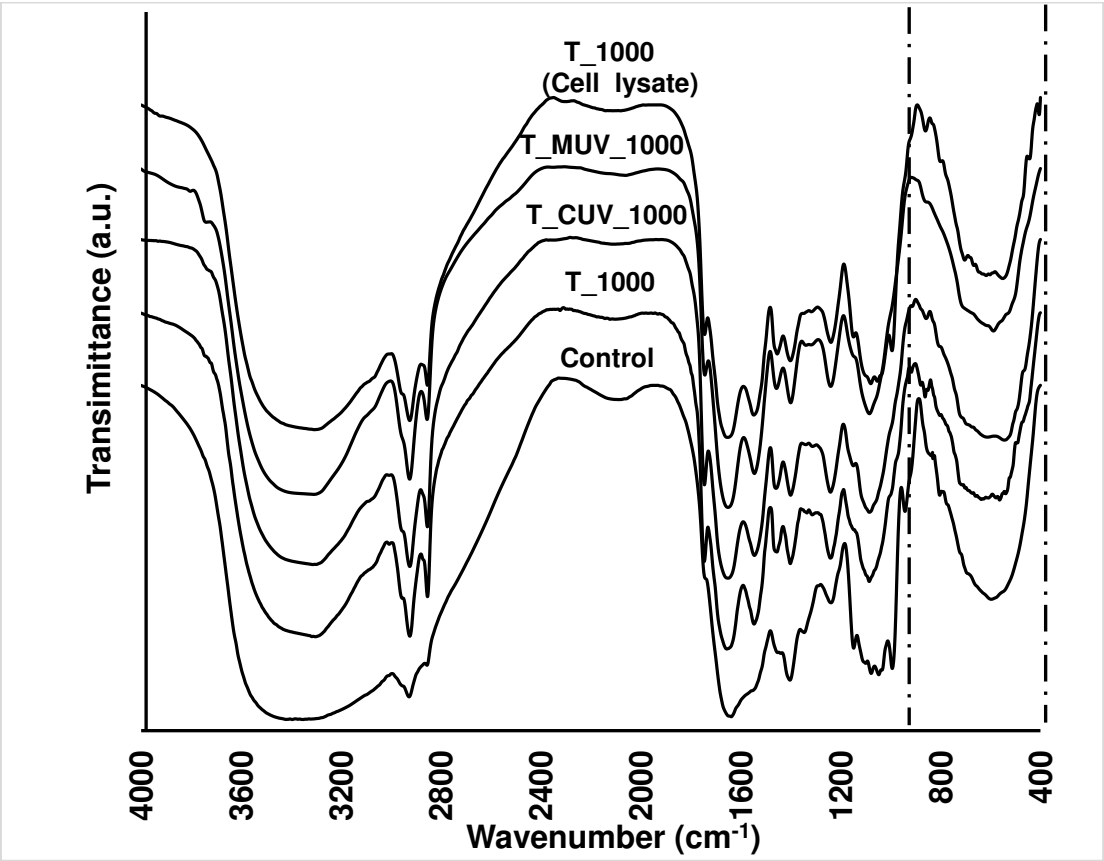
T_1000
(Cell lysate)
T_MUV_1000
T_CUV_1000
T_1000
Control
Transimittance (a.u.)
4000
3600
3200
2800
2400
2000
1600
1200
800
400
Wavenumber (cm-1)

Fig. 2

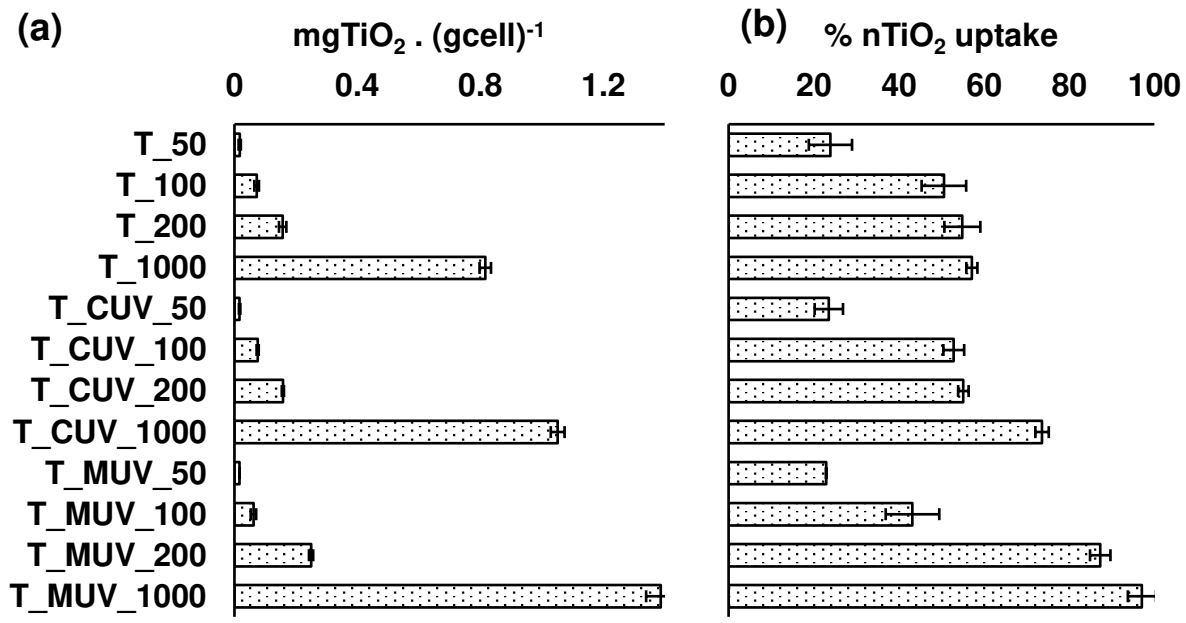
(a)
mgTiO2 . (gcell)-1
0
0.4
0.8
1.2
(b)
% nTiO2 uptake
0
20
40
60
80
100
T_50
T_100
T_200
T_1000
T_CUV_50
T_CUV_100
T_CUV_200
T_CUV_1000
T_MUV_50
T_MUV_100
T_MUV_200
T_MUV_1000

Fig. 3

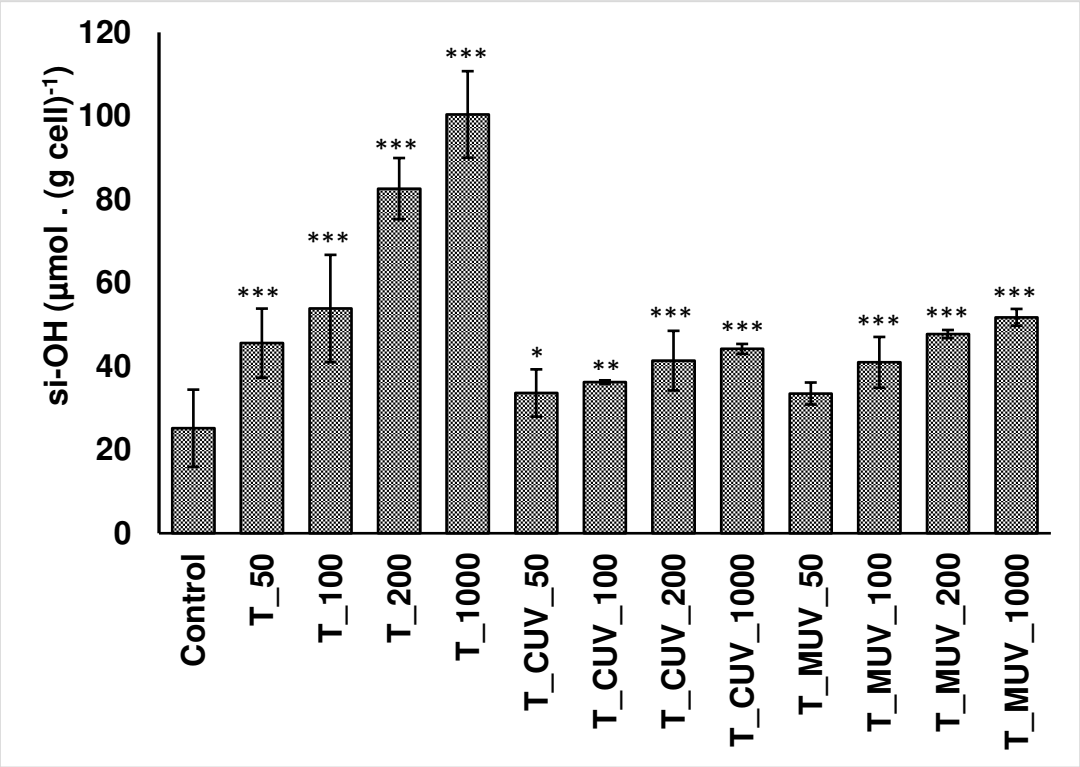
si-OH (µmol . (g cell)-1)
120
100
80
60
40
20
0
***
***
***
***
*
**
***
***
***
***
***
Control
T_50
T_100
T_200
T_1000
T_CUV_50
T_CUV_100
T_CUV_200
T_CUV_1000
T_MUV_50
T_MUV_100
T_MUV_200
T_MUV_1000

Fig. 4

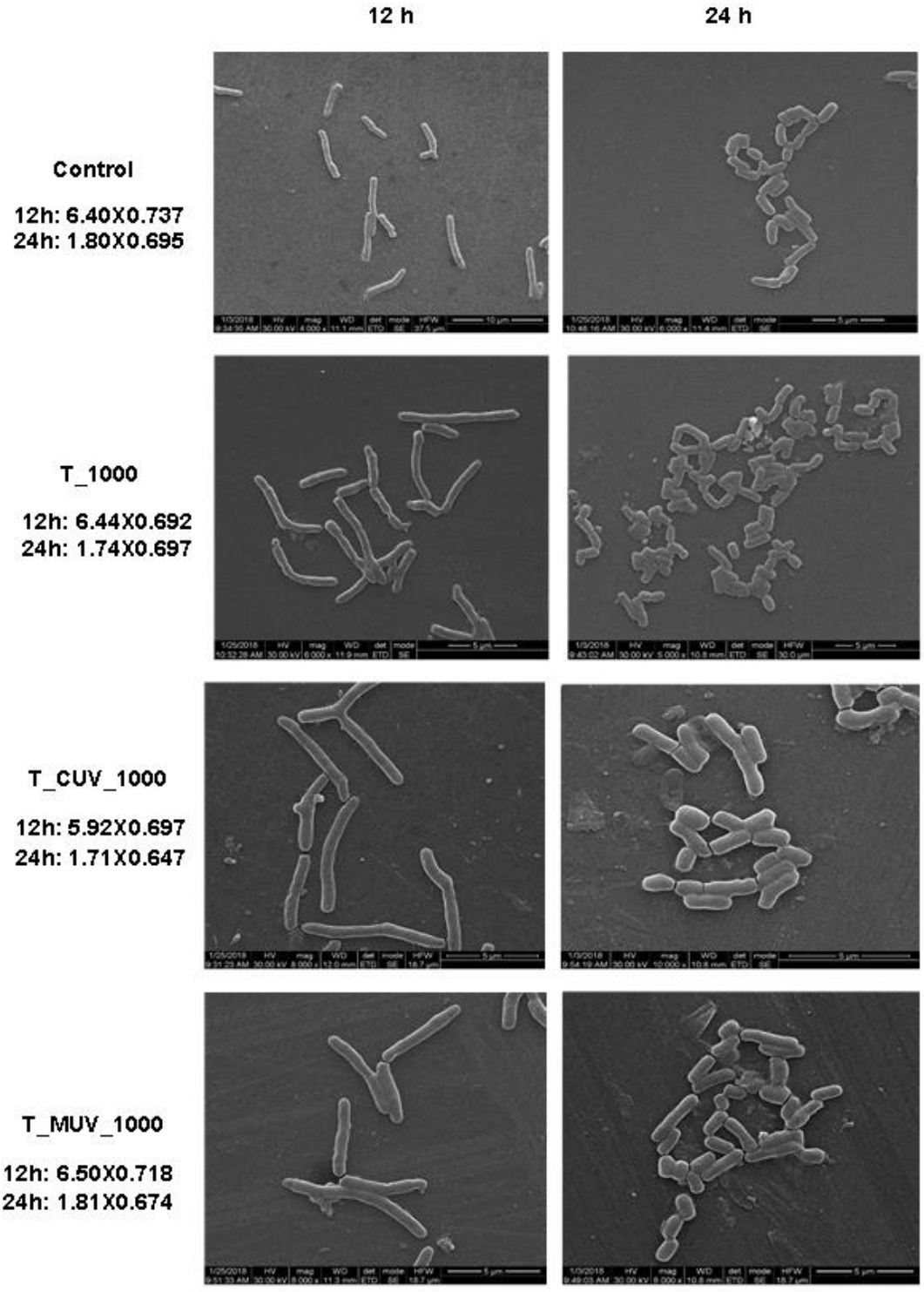
12 h
24 h
Control
12h: 6.40X0.737
24h: 1.80X0.695
T_1000
12h: 6.44X0.692
24h: 1.74X0.697
T_CUV_1000
12h: 5.92X0.697
24h: 1.71X0.647
T_MUV_1000
12h: 6.50X0.718
24h: 1.81X0.674

Fig. 5

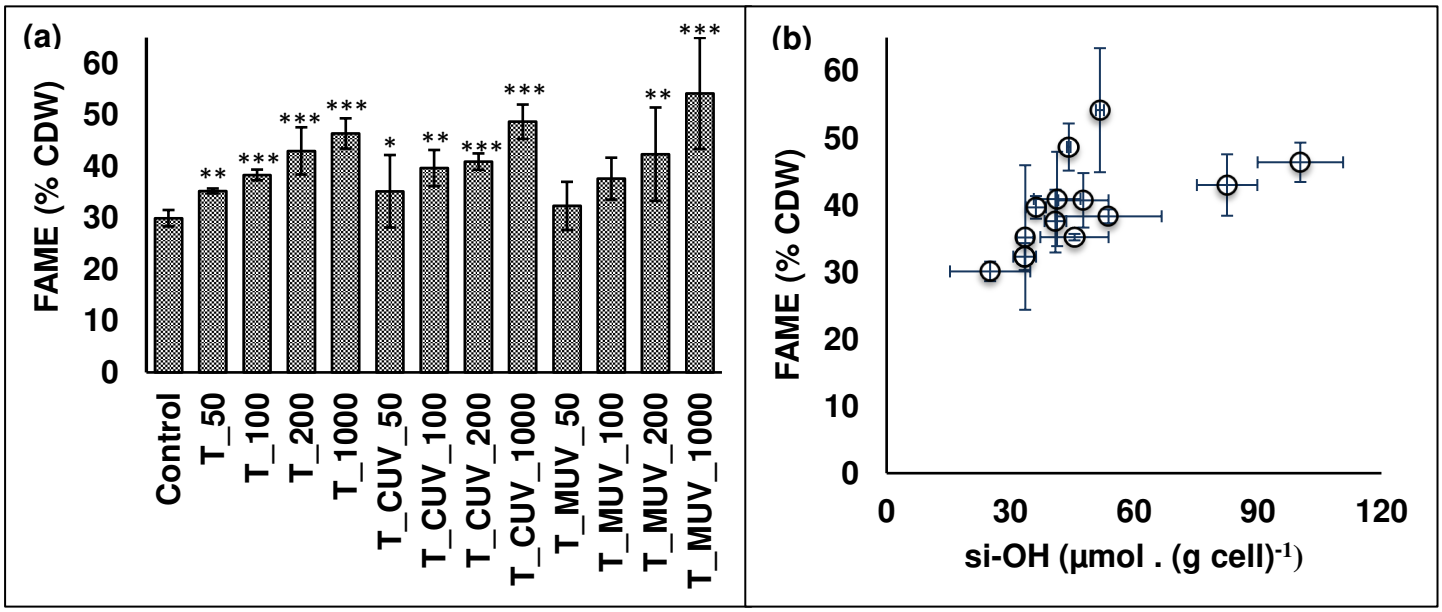
(a)
FAME (% CDW)
60
50
40
30
20
10
0
**
***
***
***
*
**
***
***
**
***
Control
T_50
T_100
T_200
T_1000
T_CUV_50
T_CUV_100
T_CUV_200
T_CUV_1000
T_MUV_50
T_MUV_100
T_MUV_200
T_MUV_1000
(b)
FAME (% CDW)
60
50
40
30
20
10
0
0
30
60
90
120
si-OH (µmol . (g cell)-1)

Fig. 6

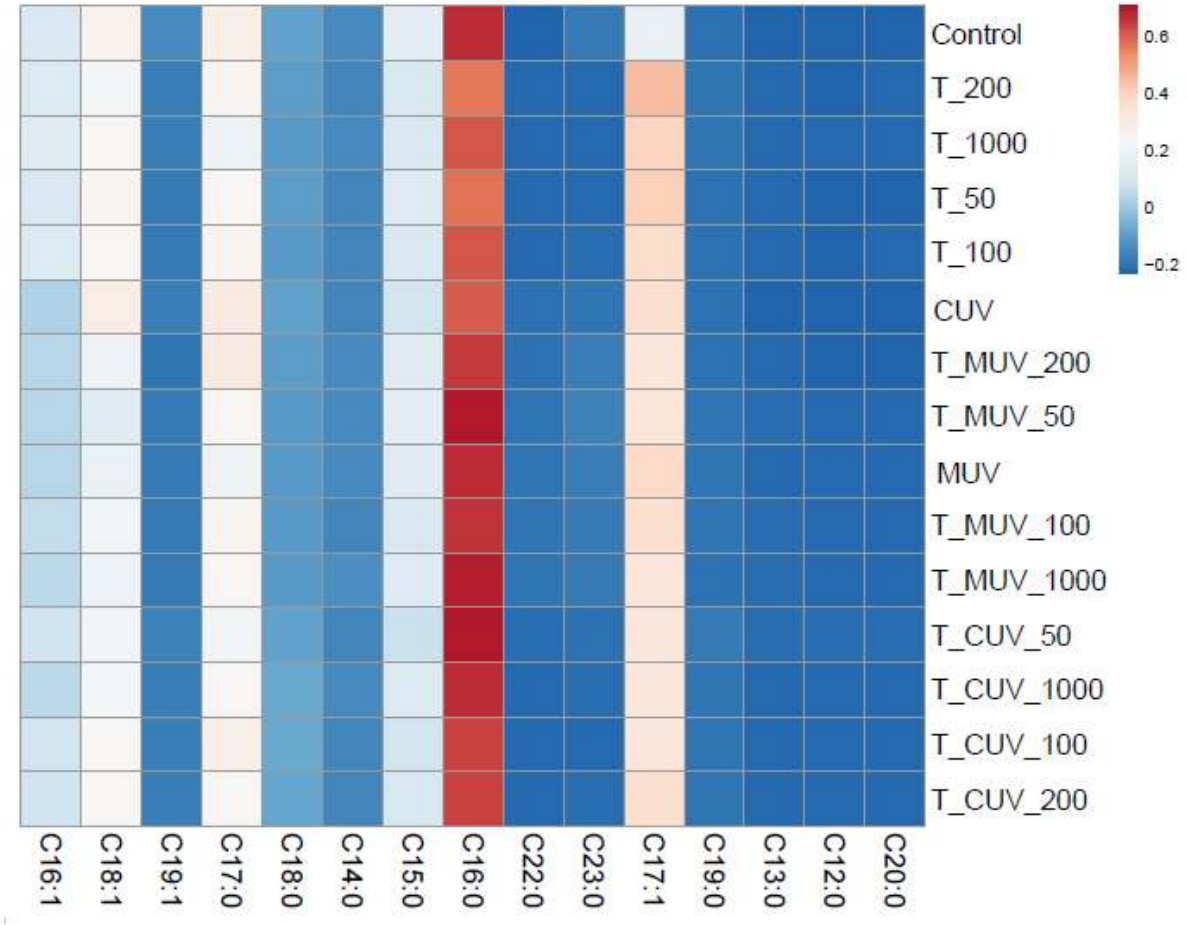
Control
T_200
T_1000
T_50
T_100
CUV
T_MUV_200
T_MUV_50
MUV
T_MUV_100
T_MUV_1000
T_CUV_50
T_CUV_1000
T_CUV_100
T_CUV_200
C16:1
C18:1
C19:1
C17:0
C18:0
C14:0
C15:0
C16:0
C22:0
C23:0
C17:1
C19:0
C13:0
C12:0
C20:0
0.6
0.4
0.2
0
−0.2

Fig. 7

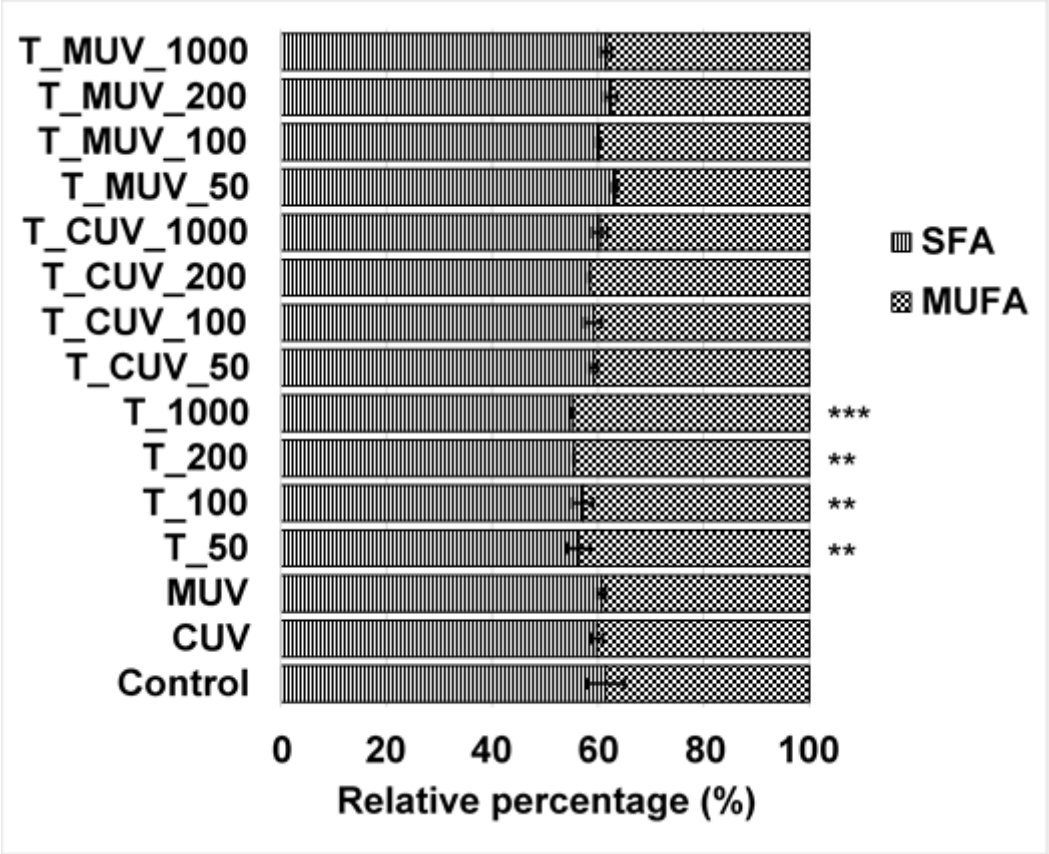
T_MUV_1000
T_MUV_200
T_MUV_100
T_MUV_50
T_CUV_1000
T_CUV_200
T_CUV_100
T_CUV_50
T_1000
T_200
T_100
T_50
MUV
CUV
Control
***
**
**
**
SFA
MUFA
0
20
40
60
80
100
Relative percentage (%)

Study medium	$nTiO_2$ ($\mu g\ L^{-1}$)	Light Condition
Control	0	Dark
CUV	0	UVB exposure throughout the study period (Continuous UV)
MUV	0	UVB exposure from mid log phase of growth (10^{th} h)
T_50	50	Dark
T_100	100	
T_200	200	
T_1000	1000	
T_CUV_50	50	UVB exposure throughout the study period (Continuous UV)
T_CUV_100	100	
T_CUV_200	200	
T_CUV_1000	1000	
T_MUV_50	50	UVB exposure from mid log phase of growth (10^{th} h)
T_MUV_100	100	
T_MUV_200	200	
T_MUV_1000	1000	

Table 1: Details of different study medium used in the study

Fatty acid chain	Compound
C12:0	Methyl Laurate
C13:0	Methyl Tridecanoate
C14:0	Methyl myristate
C15:0	Methyl pentadecanoate
C16:0	Methyl Palmitate
C16:1	Methyl palmitoleate (*cis*-9)
C17:0	Methyl margarate
C17:1	Methyl heptadecenoate (cis 8)
C18:0	Methyl stearate
C18:1	Methyl oleate(*cis*-9)
C19:0	Methyl nonadecanoate
C19:1	Methyl nonadecanoate (Trans-10)
C20:0	Methyl arachidate
C22:0	Methyl Behenate
C23:0	Methyl tricosanoate

Table 2: Fatty acid profile of biodiesel obtained from the bacterium, *R. opacus* PD630